Mon. Not. R. Astron. Soc. **000**, 1–10 (2007) Printed 24 August 2008 (MN LaTeX style file v2.2)

GD 552: a cataclysmic variable with a brown dwarf companion?

E. Unda-Sanzana[1], T. R. Marsh[2], B. T. Gänsicke[2], P. F. L. Maxted[3], L. Morales-Rueda[4], V. S. Dhillon[5], T. D. Thoroughgood[5], E. Tremou[6], C. A. Watson[5], R. Hinojosa-Goñi[1]

[1] *Instituto de Astronomía, Universidad Católica del Norte, Antofagasta, Chile; eundas@almagesto.org; rhg002@ucn.cl*
[2] *Dept. of Physics, University of Warwick, Coventry, United Kingdom CV4 7AL; t.r.marsh@warwick.ac.uk; boris.gaensicke@warwick.ac.uk*
[3] *Dept. of Physics and Astronomy, Keele University, Keele, Staffordshire ST5 5BG, United Kingdom; pflm@astro.keele.ac.uk*
[4] *Dept. of Astrophysics, University of Nijmegen, 6500 GL Nijmegen, The Netherlands; lmr@astro.ru.nl*
[5] *Dept. of Physics and Astronomy, University of Sheffield, Sheffield S3 7RH, United Kingdom; vik.dhillon@sheffield.ac.uk, C.Watson@sheffield.ac.uk*
[6] *Dept. of Physics, Sect. of Astrophysics, Astronomy & Mechanics, Univ. of Thessaloniki, 541 24 Thessaloniki, Greece; etremo@physics.auth.gr*

arXiv:0806.4892v1 [astro-ph] 30 Jun 2008

Accepted . Received ; in original form

ABSTRACT

GD 552 is a high proper motion star with the strong, double-peaked emission lines characteristic of the dwarf nova class of cataclysmic variable star, and yet no outburst has been detected during the past 12 years of monitoring. We present spectroscopy taken with the aim of detecting emission from the mass donor in this system. We fail to do so at a level which allows us to rule out the presence of a near-main-sequence star donor. Given GD 552's orbital period of 103 minutes, this suggests that it is either a system that has evolved through the ~ 80-minute orbital period minimum of cataclysmic variable stars and now has a brown dwarf mass donor, or that has formed with a brown dwarf donor in the first place. This model explains the low observed orbital velocity of the white dwarf and GD 552's low luminosity. It is also consistent with the absence of outbursts from the system.

Key words: binaries: close – binaries: spectroscopic – stars: individual: GD 552 – accretion

1 INTRODUCTION

GD 552 is a blue, high proper motion star ($0.18''$/yr) discovered by Giclas et al. (1970). It was first observed spectroscopically by Greenstein & Giclas (1978), who found that it is a cataclysmic variable star (CV) in which a white dwarf accretes matter from a low-mass companion (often termed primary and secondary star, respectively). GD 552's proper motion and position close to the plane of the Galaxy (galactic latitude 4°), combined with its blue colour all suggest that it is relatively close by. Greenstein & Giclas (1978) suggest a distance of ~ 70 pc which gives a transverse motion which is reasonable for a member of the Galactic disk, and combined with its magnitude $V = 16.5$, suggests $M_V \sim 12.5$, the equivalent of a $0.6\,\mathrm{M}_\odot$ white dwarf with a temperature of only 9000 K. The probable low luminosity of GD 552, which is of central importance to this paper, is backed up by an absence of any observed outbursts, suggesting that it may very rarely or never have outbursts (Cannizzo 1993).

The main spectroscopic study of GD 552 so far has been carried out by Hessman & Hopp (1990) (hereafter HH1990) who determined the orbital period of GD 552 of 102.7 min. They observed an extreme Balmer decrement (Hα:Hβ= 6.2:1.0), indicative of a cool, optically thin disc, another indication of low luminosity (Williams & Shipman 1988). HH1990 measured the white dwarf's projected orbital velocity to be $K_1 = 17 \pm 4\,\mathrm{km\,s^{-1}}$. This is a very low value suggestive of a low inclination system, since for edge-on systems with orbital periods similar to GD 552 K_1 is typically $\sim 60 - 80\,\mathrm{km\,s^{-1}}$. However, the emission lines from the accretion disc suggest instead a moderately inclined system as they display clearly separated double-peaks (which come from the outer disc, Horne & Marsh 1986) with velocities of $\pm 450\,\mathrm{km\,s^{-1}}$ which can be compared to typical peak velocities of $\sim 600\,\mathrm{km\,s^{-1}}$ for edge-on systems. To solve this conundrum, HH1990 suggested that the white dwarf in GD 552 is unusually massive – close to the Chandrasekhar limit in fact – allowing a low orbital inclination ($\sim 20^\circ$) and therefore the small K_1 value at the same time as large disc velocities. HH1990 were forced to their model because they assumed that the companion to the white dwarf had to be a main-sequence star. Since the companion fills its Roche lobe, Roche geometry and the orbital period uniquely specify its

density ($36.5\,\mathrm{g\,cm^{-3}}$), which, if it is a main-sequence star, also fixes its mass, which turns out to be $M_2 \sim 0.13\,\mathrm{M}_\odot$. This would cause a much larger K_1 than observed, unless the inclination is low.

More recent theoretical work has revised HH1990's estimate a little to $M_2 \sim 0.15\,\mathrm{M}_\odot$ from GD 552's orbital period (Kolb & Baraffe 1999), but the problem is qualitatively unchanged. However, this work also suggests a very different scenario. Cataclysmic variables at long orbital periods are thought to evolve towards shorter periods until the companion becomes degenerate at a period near 70 minutes. After this time, the mass donor increases in size as it loses mass and the orbital period lengthens (e.g. Howell, Nelson & Rappaport, 2001; Kolb 1993). Thus although if GD 552 is approaching the period minimum its donor mass must be $M_2 \sim 0.15\,\mathrm{M}_\odot$, if it has already passed the minimum and is now evolving to longer periods, it would be about a factor of four times less massive, and there would be no need for HH1990's massive white dwarf, face-on model. Moreover, such a system would have an extremely low mass transfer rate, consistent with GD 552's lack of outbursts and probably low intrinsic luminosity. The evolution just described is the standard explanation for the observed minimum orbital periods of CVs, which however fails on two counts. First, the observed minimum around 80 min is distinctly longer than the theoretical value of 70 min (Kolb & Baraffe 1999; although Willems et al. (2005) propose that the period minimum might be longer than expected because of extra angular momentum loss from circumbinary disks), and, second, while we expect most systems to have passed the period minimum there is just one single well-established example of such a system known (SDSS 103533.03+055158.4, Littlefair et al. 2006) although there are a few other good candidates (Mennickent et al. 2001; Littlefair, Dhillon & Martin 2003; Patterson, Thorstensen & Kemp 2005; Araujo-Betancor et al. 2005; Southworth et al. 2006). Therefore it is of considerable interest to establish whether GD 552 is a pre- or post-period-minimum system.

In this article we carry out a test to distinguish between the two models of GD 552. If the pre-period-bounce model is correct, then, as we show in this paper, we should be able to detect features from the M star in a low mass-transfer rate system such as GD 552. If, conversely, the post-period-bounce model is correct, the donor will be extremely faint and it should not be detectable. In summary, our task is to set the strongest possible limit upon the presence of a hypothetical M dwarf such that we can say that we would have seen it had GD 552 been a pre-bounce system.

2 OBSERVATIONS AND DATA REDUCTION

We carried out observations of GD 552 in January and August 2001 on the island of La Palma in the Canary Islands (see Table 1 for details). In January 2001, the 2.5-m Isaac Newton Telescope (INT) was used in conjunction with the Intermediate Dispersion Spectrograph (IDS) to acquire one dataset. Another dataset obtained in January 2001 used the 4.2-m William Herschel Telescope (WHT) in conjunction with the double-beamed high-resolution ISIS spectrograph. In August 2001 only WHT/ISIS was used. The weather was good during both runs, with no clouds and a typical seeing of 1 arcsecond.

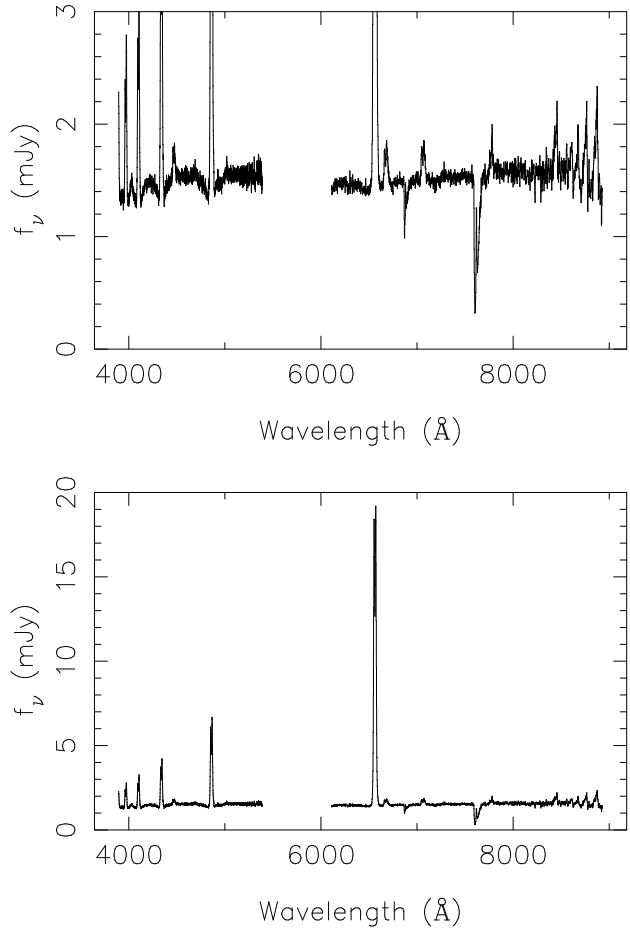

Figure 2. Low resolution spectra acquired in January 2005. The upper panel is a vertical enlargement of the lower one. Note the broad absorption wings around the emission lines.

An additional low-resolution spectrum was acquired on January 4, 2005, again with WHT/ISIS (see Table 1 for details). This spectrum was acquired with a vertical slit in order to obtain approximately correct relative fluxes. It was calibrated using observations of Feige 34 (Oke 1990). The seeing on this night was around 2.5" and variable and so the flux calibration is only approximate. See Table 1 for details.

We flux calibrated the earlier spectra using observations of the spectrophotometric standard HD19445 which we also used to remove the effect of telluric lines on the red data (Bessell 1999). Flat-fields and comparison arc spectra were taken at regular intervals (every $\sim 60\,\mathrm{min}$).

The spectra were optimally extracted (Marsh 1989), with flat fields interpolated from the many ones taken during the night. The wavelength scales for each science spectrum were obtained by interpolating the solutions of the nearest two arc spectra. For the January 2001 datasets a comparison star was included in the slit. In this case slit losses were corrected using the ratio of the spectra of the comparison star to a spectrum taken with a wide slit close to the zenith. For the August 2001 datasets no comparison star was observed, so we simply normalised the continua of these spectra.

Six images were acquired with the WHT on 25 Septem-

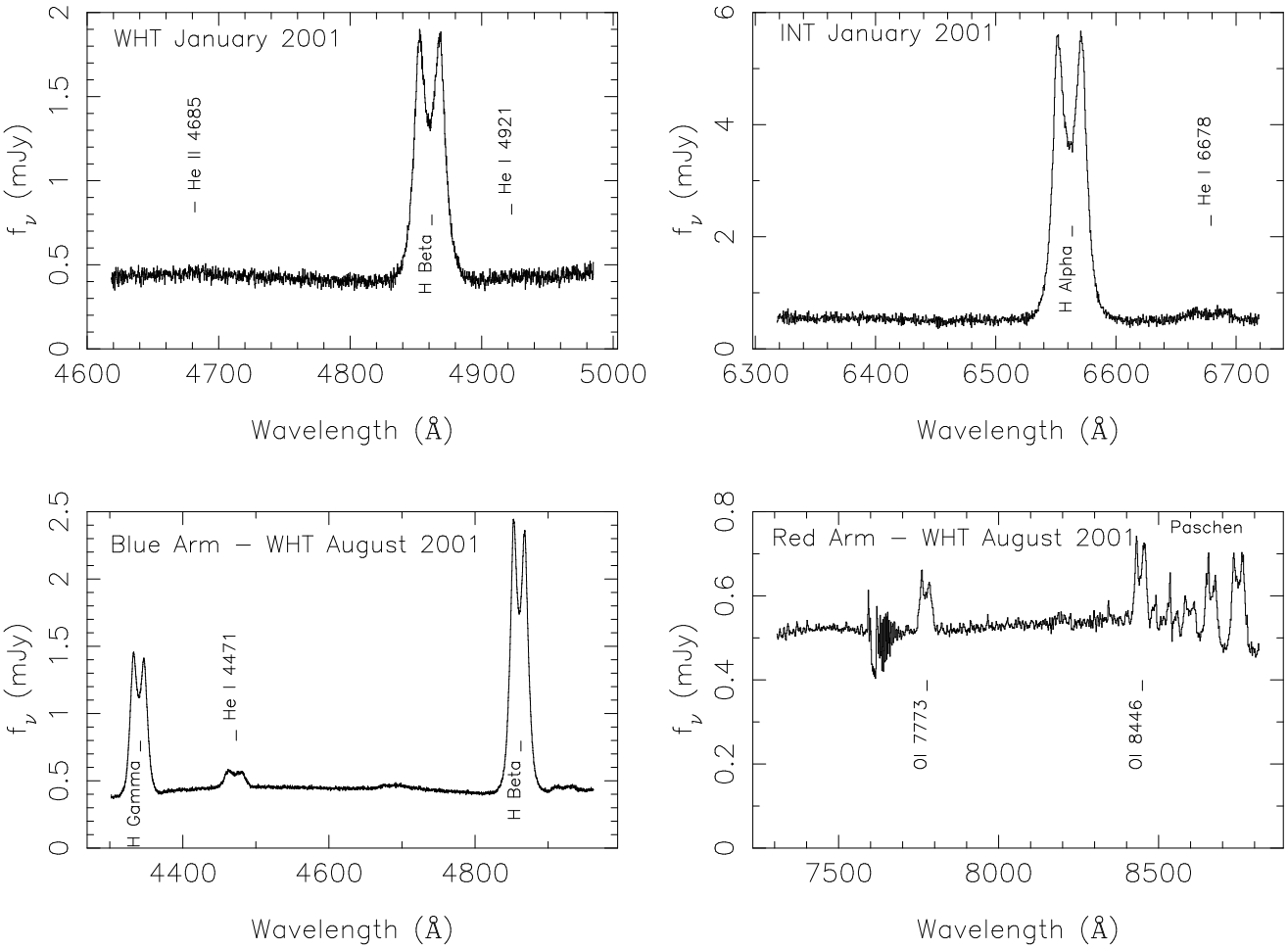

Figure 1. Average spectra for the high-resolution datasets. A correction for telluric absorption has been made to the I-band spectra, although the very heavy absorption at 7600 Å could not be successfully removed.

ber 2006 using a Harris I-band filter. One Landolt standard (Mark A1) with very similar airmass was observed to flux calibrate the images. Observations from the nearby Carlsberg Automatic Meridian Circle[1] on the same night show that the night was mostly photometric with normal extinction.

Finally, 5.4h of filterless CCD photometry of GD552 was obtained on 29 July 2005 using a SI-502 516×516 pixel camera on the 1.2m telescope at Kryoneri Observatory. The data were reduced using the pipeline described in Gänsicke et al. (2004), where we used USNO-A2.0 1500-09346766 (located $\sim 1'$ north-east of GD552, $B = 16.8$, $R = 15.6$) as comparison star.

Ultraviolet STIS spectroscopy of GD552 was retrieved from the HST archive. The system was observed with the far-ultraviolet (FUV) G140L grating and the $52'' \times 0.2''$ aperture on 24 October 2002 for a total of ~ 4 h. The observation was split into 15 individual exposures of 970 s each. An additional three 1410 s near-ultraviolet spectra using the G230LB grating were obtained on 31 August 2002, again using the $52'' \times 0.2''$ aperture.

[1] http://www.ast.cam.ac.uk/∼dwe/SRF/camc_extinction.html

3 ANALYSIS

3.1 Average profiles and trailed spectra

Figure 1 shows average spectra for our data. Figure 2 shows the available low resolution spectra. We observe double peaked profiles in all the detected lines: He I 4471.68 Å (hereafter He I 4471), He II 4685.750 Å (hereafter He II), He I 4921.93 Å (hereafter He I 4921), He I 6678.15 Å (hereafter He I 6678), O I 7773, O I 8446 and the Paschen and Balmer series. In the general theory of CVs, the double peaked profiles are consistent with disc emission.

A second order polynomial was fitted to the continuum of each dataset and then the data were divided by these fits. The normalised continua were subtracted, and the datasets were binned in 20 (Jan) or 30 (Aug) orbital phase bins before plotting Figure 3. These trailed spectra display double peaked emission following a sinusoidal motion with orbital phase. We interpret this as the rotating accretion disk, approximately tracking the emission of the white dwarf it surrounds. The other remarkable feature in these spectra is a higher-amplitude sinusoid also varying with orbital phase, but shifted with respect to the assumed zero phase. It can be seen very clearly, for instance, in O I 7773 (Figure 3). This emission is produced in the stream/disc impact region,

Table 1. Summary of the WHT and INT spectroscopic data used in the analysis. In this table MD stands for 'mean dispersion'. FWHM is the full width at half maximum of the unblended arc lines. T is the mean exposure time per frame and DT is the average dead time between exposures. N is the number of spectra collected per night per arm.

Telescope/ Instrument	CCD/Grating	Date	Start - End (UT)	Orbits covered	λ range (Å)	MD (Å pixel^{-1})	FWHM (Å)	T/DT (s)	N
INT/IDS	EEV10/R1200B	12/13 Jan 2001	19:48-22:06	1.343	6318-6719	0.39	0.78	300/30	26
WHT/ISIS	EEV12/H2400B	12/13 Jan 2001	19:52-21:13	0.788	4618-4985	0.21	0.42	300/12	32
WHT/ISIS	EEV12/R1200B	13/14 Aug 2001	23:28-05:34	2.979	4301-4962	0.22	0.69	290/16	61
WHT/ISIS	TEK4/R316R	13/14 Aug 2001	23:35-05:34	2.911	7306-8814	1.48	3.43	300/5	63
WHT/ISIS	EEV12/R1200B	04/05 Jan 2005	19:50-19:58	0.081	3900-5390	0.88	1.8	500/0	1
WHT/ISIS	TEK4/R316R	04/05 Jan 2005	19:50-19:58	0.081	6110-8930	1.65	3.2	500/0	1

which is usually termed the bright spot. Note that the phasing of this sinusoidal is different for the January and August datasets. This is due to the uncertainty in the zero phase of the ephemeris used to fold the data (HH1990's).

Using the average of the WHT spectra acquired in January 2005, we measured the Balmer decrement defined as the ratio of line fluxes H α : H β : H γ. We did this by integrating the flux from each profile after subtracting a low order fit to the continua. We computed H α : H β : H γ = 2.0 : 1.0 : 0.56. Our values for the Balmer decrement differ noticeably from HH1990's (H α : H β : H γ = 6.2 : 1.0 : 0.26), being rather closer to Greenstein & Giclas (1978) (H α : H β : H γ = 2.2 : 1.0 : 0.5). Qualitatively, though, our conclusion is the same: the Balmer decrements suggest that the accretion disk is optically thin and cool (see, for example, Williams & Shipman, 1988). This conclusion is strengthened by the detection of O I 7773 which, according to Friend et al. (1988) is a good indicator of the state of the disc, its emission indicating an optically thin accretion disc.

3.2 The primary star

HH1990 measured a value of $17 \pm 4\,\mathrm{km\,s^{-1}}$ for K_1. We tried to check and refine this value by using Schneider & Young (1980)'s method. We convolved our data with a difference of Gaussians equidistant from a candidate line centre, and define the velocity as the displacement of the double Gaussians such that the convolution equals zero. By increasing the separation of the Gaussians we gather information from the wings of the profile, which is produced in regions of the disc closer to its centre (Horne & Marsh 1986). We assume that the motion of these regions tracks the motion of the accreting object, so the further into the wings the measurement is made, the better the estimate of the motion of the white dwarf. The process does not continue indefinitely because there is a maximum velocity in the line wings, which corresponds to the Keplerian motion of the innermost ring of gas just before settling onto the white dwarf. However, in practice, before reaching this limit the reliability of the calculation is constrained by the noise present at the continuum level.

The motion of each disc region is calculated by fitting the orbital solution:

$$V = \gamma - K \sin\left(\frac{2\pi(t - t_0)}{P}\right) \quad (1)$$

to the measurements. γ is the systemic velocity, K is the velocity of the source of the emission, t_0 is the time of superior conjunction of the emission-line source, and P is the orbital period of the system. Further, we avail ourselves of a diagnostic diagram (Shafter, Szkody & Thorstensen 1986) to decide when the calculation is becoming dominated by noise as the separation of Gaussians (a) increases. This should reveal itself as a sharp rising of the statistics σ_K/K. At the same time, we also expect to see convergence of the calculated parameters (K, γ) and a phasing appropriate to the white dwarf.

In our diagrams (Fig. 4) we do not put a strong constraint on the value of convergence for the phasing (bottom panels) because the ephemeris of this system has a large uncertainty and thus its orientation is arbitrary for the date of our observation. For a larger than $2500\,\mathrm{km\,s^{-1}}$ the noise dominates both diagrams so this is the upper limit for the abscissa in our plots. The H β diagram displays a reasonable degree of convergence when a approaches $2000\,\mathrm{km\,s^{-1}}$. On reaching that value the noise takes off. On the other hand, for large values of a in H α we are picking data contaminated by the wings of He I 6678 and thus we do not expect a clear convergence in this diagram, although the noise seems to dominate once a reaches $2200\,\mathrm{km\,s^{-1}}$. Eventually, as it is not obvious which value to favour in H α we take as K_1 the value of K for $a = 1900\,\mathrm{km\,s^{-1}}$ in H β, right before the noise begins to dominate. This is $14.1 \pm 2.7\,\mathrm{km\,s^{-1}}$ consistent with HH1990. The uncertainties were estimated by means of the bootstrap method, repeating the calculation for 10000 bootstrap samples (Diaconis & Efron 1983).

The high resolution B-band spectrum of Fig. 1 shows signs of broad absorption wings flanking the Balmer lines. These are often seen in low luminosity dwarf novae (e.g. Szkody et al. 2007) and originate in the photosphere of the white dwarf. Low resolution spectra taken in January 2005 and September 2006 confirm the presence of the white dwarf photospheric lines (Fig. 2). The white dwarf is also revealed in HST/STIS ultraviolet spectra through the a very broad L α feature extending to 1600A (Fig. 6). This feature, which results from L α from neutral hydrogen plus quasi-molecular features at 1400 and 1600 Å from H_2^+ and H_2, is a hallmark of cool white dwarfs.

For the purpose of the spectral analysis, we have computed a grid of white dwarf models covering effective temperatures in the range 8000 K–15 000 K and surface gravities of $\log g$ = 7.5, 8.0, and 8.5 using the stellar atmosphere and spectral synthesis codes TLUSTY/SYNSPEC (Hubeny & Lanz 1995). Metal abundances were set to 0.1

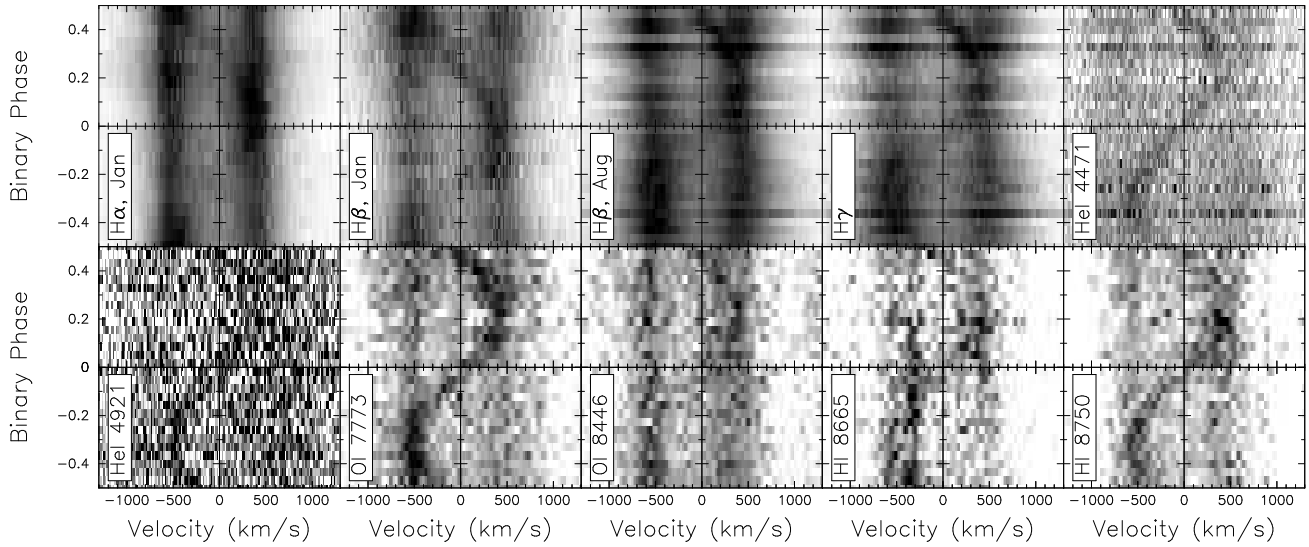

Figure 3. Phase binned data. The fluxes in this figure have been normalised by the maximum value the flux reaches for each wavelength. We set the colour scale to white for 0 flux and to black for 85% of this normalised flux, with the exception of line He I 4921for which black corresponds to 40% of the normalised flux.

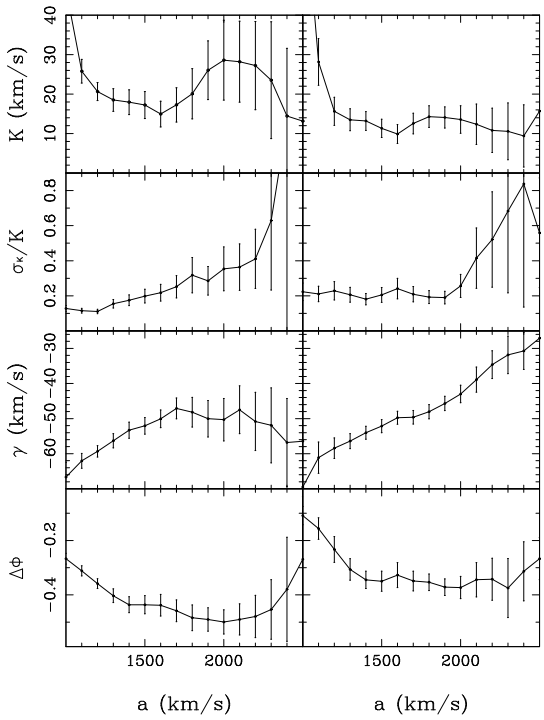

Figure 4. Diagnostic diagram for H α (left) and H β (right), using INT January 2001 and WHT August 2001 data respectively.

times their solar values, as suggested by the weakness of the Mg$\lambda\lambda$2796,2803 resonance doublet. The assumed value for the metal abundance is within the typical range for CVs (Sion & Szkody 2005). A first exploratory fit revealed that none of the white dwarf model spectra could reproduce the STIS data alone, as the flux of the model spectra rapidly drops to zero shortward of $\sim$ 1300 Å, in contrast to the observed spectrum that has a substantial non-zero flux down to 1150 Å. Moreover, it turns out that the 15 individual far-ultraviolet spectra show substantial flux variability, supporting the presence of a second (variable) component. The ultraviolet flux variability shows a clear dependence on wavelength, and we have fitted the continuum slope of the spectrum with a linear slope, $F_\lambda = 7.22 \times 10^{-19}\lambda - 5.9 \times 10^{-16}\,\mathrm{erg\,cm^{-2}s^{-1}\AA^{-1}}$. Qualitatively, such a slope is what could be expected from either an optically thin emission region (where absorption is dominated by bound-free absorption) or an optically thick relatively cool quasi-blackbody component (where the far-ultraviolet emission is on the Wien part of the blackbody spectrum). We then explored two-component fits to the STIS data consisting of this linear slope plus a white dwarf model, with the contributions of the slope and the white dwarf being normalised to match the observed continuum below 1300 Å and in the range 1580–1620 Å, respectively. The best fit for $\log g = 7.5$ is shown in Fig. 5 (left panel). This simple model provides a surprisingly good match to the STIS spectrum over the entire ultraviolet range. However, an extrapolation of this simple linear slope over a broader wavelength range, i.e. into the optical, is not warranted, as the exact nature of this emission component is not known.

The parameters determined from the fit are the white dwarf effective temperature $T_{\rm eff}$, and the flux scale factor between the synthetic and the observed spectrum. Assuming a white dwarf radius, the flux scaling factor can be used to calculate the distance to the system. As the white dwarf mass is unconstrained by this analysis, we ran the fit for $\log g$ = 7.5, 8.0, and 8.5, corresponding to white dwarf masses and radii of (0.33 $\mathrm{M_\odot}$, 1.15×10^9 cm), (0.57 $\mathrm{M_\odot}$, 8.65×10^8 cm), and (0.9 $\mathrm{M_\odot}$, 6.15×10^8 cm), respectively (where we have assumed a Hamada-Salpeter (1961) Carbon-Oxygen core mass-radius relation). The best fit parameters for $\log g = 7.5$, 8.0, and 8.5 are (10 500 K, 125 pc), (10 900 K, 105 pc), and (11 300 K and 85 pc), respectively. Because of the very strong temperature dependence of the 1600 Å H_2^+ the STIS spectrum constrains the white dwarf temperature within a very narrow range.

Fig. 5 (right panel) shows that the white dwarf model obtained from the fit to the STIS data extended into the optical range clearly underpredicts the observed flux by $\sim 50\%$. The presence of double-peaked Balmer emission lines clearly reveals the presence of an accretion disc in the system that is contributing light in the optical. We model the accretion disc by an isobaric/isothermal hydrogen slab, which has three free parameters: the disc temperature $T_{\rm d}$, the column density Σ, and the flux scaling factor (see Gänsicke et al. 1997, 1999 for details). A disc temperature of $T_{\rm d} = 5800\,{\rm K}$ and a column density of $\Sigma = 2.3 \times 10^{-2}{\rm g\,cm^{-2}}$, scaled to the observed Hα emission line flux provides an adequate model of the optical spectrum. The emission line flux ratios of the model are $\mathrm{H}\,\alpha : \mathrm{H}\,\beta : \mathrm{H}\,\gamma = 2.2 : 1.0 : 0.56$, fairly close to the observed values (Sect. 3.1). For a distance of $\sim 100\,{\rm pc}$, the area of hydrogen slab implied by the flux scaling factor is consistent with the size of the Roche lobe of the white dwarf. The disc parameters found here are very similar to those found in a number of other studies of quiescent accretion discs in CVs (e.g. Williams 1980, Marsh 1987, Lin et al. 1988, Rodriguez-Gil et al. 2005). We refrained from more detailed modelling of the optical data as the spectrum was obtained under non-photometric conditions, and the flux calibration is subject to some uncertainty. Nevertheless the temperature derived from the UV data is consistent with our detection of the white dwarf's photosphere in our optical spectra.

The recent discovery of several non-radially pulsating white dwarfs in CVs (e.g. van Zyl et al. 2004, Warner & Woudt 2004, Araujo-Betancor et al. 2005, Patterson et al. 2005, Warner & Woudt 2005 and Gänsicke 2006) motivated the short photometric time series observation of GD552 carried out at Kryoneri observatory. Visual inspection of the light curve (Fig. 6) reveals substantial variability on time scales of tens of minutes, plus a modulation over $\sim 4.5\,{\rm h}$. A Lomb-Scargle period analysis (Lomb 1976, Scargle 1982) shows no substantial power at periods shorter than $\sim 15\,{\rm min}$, where non-radial pulsations would be expected to show up. The conclusions from this admittedly limited set of data is that the white dwarf in GD 552 is probably too cool to drive ZZ Ceti pulsations in its envelope and the varibility seen in the light curve is probably due to flickering in the accretion disc.

3.3 The secondary star

The presence of a secondary star (assumed to be an M dwarf since we are testing for the presence of a star of mass $0.15\,{\rm M}_{\odot}$) is not obvious either in the average or in the trailed spectra.

Our main aim was to detect photospheric absorption lines, especially the NaI doublet near 8200 Å which is strong in late M dwarfs. To do so we compared our GD 552 spectra with a set of M dwarf template spectra kindly provided by Kelle Cruz (personal communication) following the classification by Kirkpatrick, Henry & McCarthy (1991). The stars used are listed in Table 2.

The Na I doublet near 8200 Å and nearby molecular bands are the fingerprints of M dwarfs. As we were not able to recognise any such features in the GD 552 data, we looked for a constraint upon its presence given that its features are not detectable. First we normalised the spectra of GD 552 and of each template in Table 2. We did this by dividing by a constant fit to the continuum in the range 8100-8400 Å, excluding the ~ 8200 Å doublet. Then we subtracted each normalised template from the GD 552 data in 5% steps. In Figure 7 we show an example of this procedure. GD 552 is at the bottom of the plot. Each profile above GD 552 increases the amount of template subtracted from the data by 5%. Consistently, we found that for all the templates the presence of M star features is obvious once we reach 10%.

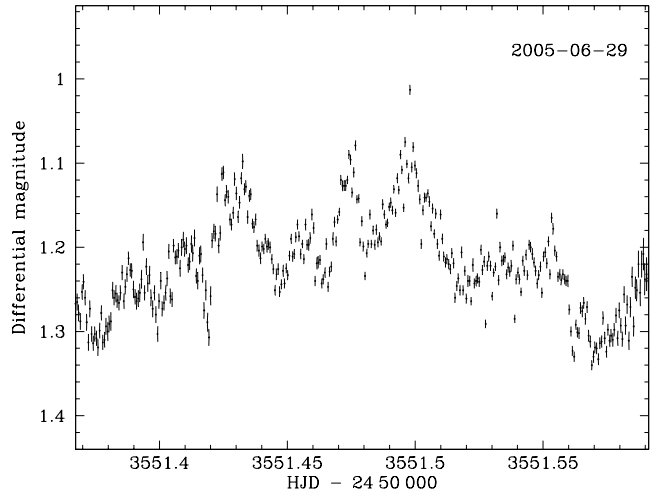

Figure 6. Kryoneri CCD photometry of GD 552.

Table 2. List of M star templates used for estimating maximum contribution of an M star to the GD 552 profile.

Spectral Type	Star
M0.5	Gl 720A
M1	Gl 229
M1.5	Gl 205
M2.5	Gl 250B
M3	Gl 752A
M3.5	Gl 273
M4	Gl 213
M4.5	Gl 83.1
M5.5	Gl 65A
M6	Gl 406
M6.5	G 51-15
M7	VB 8
M8	VB 10
M9	LHS 2065

3.4 System parameters

In section 3.3 we placed an upper limit of 10% upon the contribution of an M star to the spectrum of GD 552 in the range 8100 to 8400Å. We now use this restriction to estimate the mass of this hypothetical star. This will allow us to compare directly to HH1990's M_2 value, and thus to test their model.

We first need to convert our constraint into one upon the I-band magnitude of the M star. We start from the relation between magnitudes and fluxes, including a colour correction to make our data match the profile of the I band:

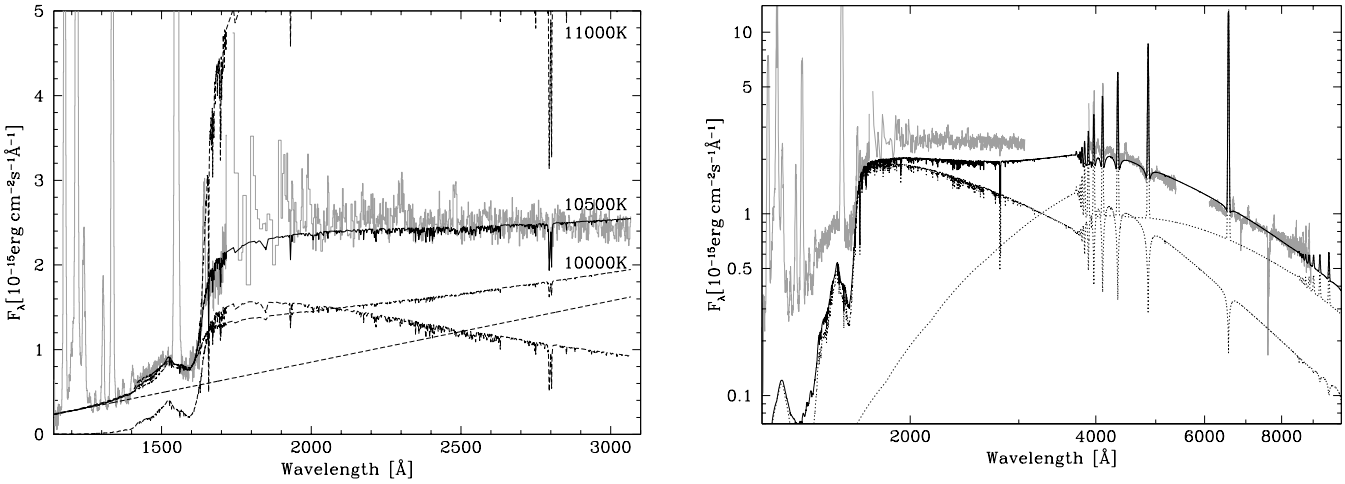

Figure 5. Left: The archival STIS ultraviolet spectrum of GD552, plotted in gray. The solid line shows a two-component fit consisting of a linear slope plus a white dwarf model spectrum ($T_{\rm eff} = 10\,500$ K, $\log g = 7.5$), both components are plotted individually as dashed lines. Shown as dotted line are the same two-component models, but for $T_{\rm eff} = 11\,000$ K (top curve) and 10 000 K (bottom curve). Right: The STIS ultraviolet spectrum along with our WHT low-resolution spectrum, plotted in gray. Plotted as solid black line is the sum of the white dwarf model as shown in the left panel plus the spectrum of an isothermal/isobaric hydrogen slab. Both model components are plotted individually as dotted lines.

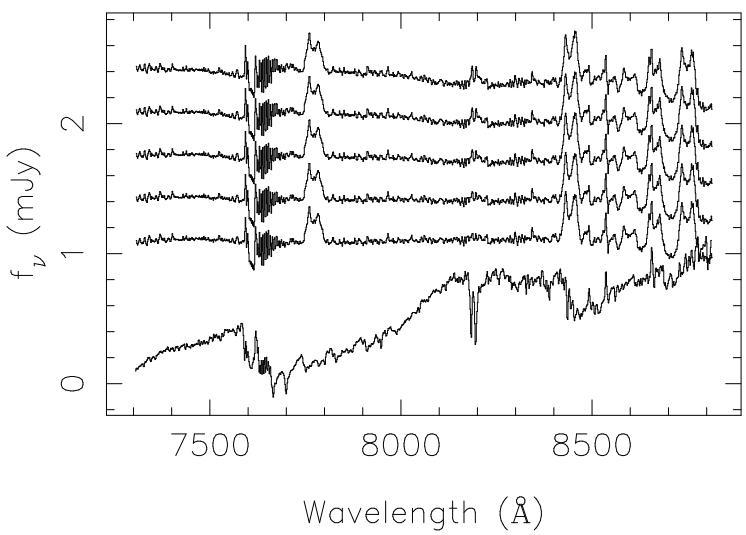

Figure 7. From bottom to top: normalised template star (Gl 65A); normalised GD 552; and the four following curves are normalised GD 552 minus 5%, 10%, 15% and 20% of the normalised template respectively. When 10% of Gl 65A is subtracted from GD 552 (third curve, top to bottom), the presence of M star features is easily seen from the growing bump at 8200Å due to the Na I doublet. The vertical scale in the figure includes an offset of 0.5 between each plot and thus it is arbitrary.

$$m_{I,10\%MS} = m_{I,GD\ 552} - 2.5\log\left(\frac{\int_{\lambda_i}^{\lambda_f}\epsilon_I\lambda f_{\lambda,10\%MS}d\lambda}{\int_{\lambda_i}^{\lambda_f}\epsilon_I\lambda f_{\lambda,GD\ 552}d\lambda}\right) \quad (2)$$

In this equation, $10\%MS$ stands for 10 percent of the template M star; ϵ_I is the transmission for the I Band; λ_i and λ_f are the limits of the observed range in wavelength. $f_{\lambda,10\%MS}$ is 10% of the normalised flux density of the M star, obtained by dividing by a constant fit to the 8100-8400 Å region (the Na I doublet at 8200 Å excluded) and multiplied by 0.10. Similarly, $f_{\lambda,GD\ 552}$ is the flux density of GD 552 calculated by dividing by a constant fit to its continuum. A field star in front of GD 552 made difficult to do this in previous years. By September 2006, however, the interloper had moved enough to make this calculation straightforward (see Figure 8). We measured $m_{I,GD552} = 16.3$ from our data. Then we use equation 2 with the M star templates listed in Table 2, obtaining $m_{I,10\%MS}$ as a (mild) function of the assumed spectral type (hereafter this will be referred to simply as m_I). In Figure 9 we compare these values after conversion to absolute magnitude M_I for distances of 70 and 125 pc with the absolute magnitudes of young M dwarfs of the same spectral type from Leggett (1992). In doing this we are assuming solar-like metallicities.

The vertical line in Figure 9 marks the spectral type for a hydrogen burning star with the lowest possible mass ($\sim 0.08\,\mathrm{M}_\odot$, Kirkpatrick & McCarthy 1994). The difference between the top and bottom panels is the distance assumed in each case. In the top panel we used the value $d \sim 70$ pc

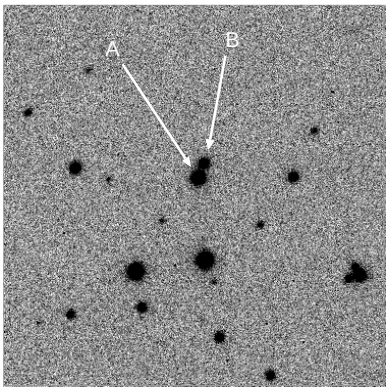

Figure 8. GD 552 (marked with an A) and a field star (marked with a B) in September 2006 (image scale is $\sim 1'$ by $1'$). The field star was in front of the system in previous years and made impossible to estimate GD 552's magnitude with any certainty. The high proper motion of GD 552 results in it and the field star now being resolved. Using our data we measured $I = 16.3$ for GD 552 and $I = 17.6$ for the field star.

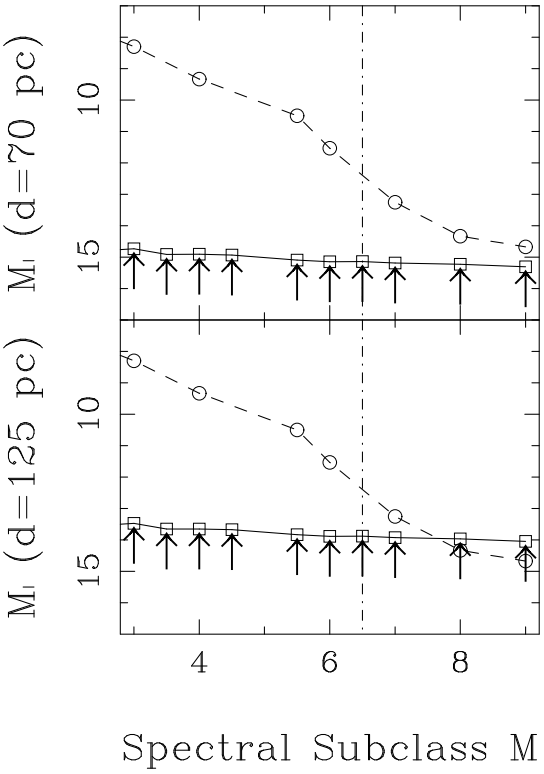

Figure 9. Comparison of the upper limit on M_I derived from our I-band spectra for the mass donor in GD 552 (solid line, open squares plus arrows, to indicate the upper-limit nature of the point) and M_I for young M dwarfs of the same spectral type (dashed line, open circles, Leggett 1992). The vertical line at M6.5 marks the limit set by Kirkpatrick & McCarthy (1994) for a hydrogen burning star. The pannels assume different distances to the system. The upper one uses the old Greenstein & Giclas (1978) value while the lower panel uses the distance estimated in this paper.

from Greenstein & Giclas (1978); it is clear from it that the absolute magnitudes allowed by our data are inconsistent with the assumption that the mass donor in GD 552 is a main-sequence star. This implies that the mass of the companion star $M_2 < 0.08 M_\odot$, ruling out near main-sequence models such as that of HH1990. Our conclusion remains unaltered even if GD 552 is at the maximum distance of 125 pc calculated for a $0.33 \mathrm{M}_\odot$ white dwarf (Section 3.2) which is lower than any white dwarf mass measured in any CV.

4 DISCUSSION

Our model of GD 552 is radically different from that of HH1990. Where they have a very high mass white dwarf in an almost face-on system, with an M dwarf donor of mass $\sim 0.15\,\mathrm{M}_\odot$, our failure to detect the mass donor requires that it is a brown dwarf with $M_2 < 0.08\,\mathrm{M}_\odot$. This makes GD 552 an excellent candidate for a post-period-bounce system with an age of about 7 Gyr (Politano et al. 1998). Our explanation of the low K_1 is therefore simply a case of extreme mass ratio, and we do not require a particularly low orbital inclination. If the secondary is low mass, there is no need for the system to be face on to get $K_1 = 17.4\,\mathrm{km\,s^{-1}}$, and therefore neither is there any need for the white dwarf to have a high mass to produce the double peaked profiles. For example, the observed value of K_1 can be matched with a white dwarf of mass $M_1 = 0.6 \mathrm{M}_\odot$ in orbit with a companion of mass $M_2 = 0.03 \mathrm{M}_\odot$ with a moderate inclination of $i \sim 60^\circ$.

Patterson et al. (2005) suggested that GD 552 is a likely "period bouncer" (post period minimum CV) because of its lack of outbursts and small K_1. We have now given support to their suggestion. However, HH1990's original model *could* have been correct and the search for the donor was a crucial step in ruling out HH1990's hypothesis. Mass donors are easily visible in other systems with hotter white dwarfs and with orbital periods similar to GD 552 (e.g. HT Cas, $P_{orb} = 106.1 min$, M5-M6V secondary spectral type, Marsh 1990; Z Cha, $P_{orb} = 107.3 min$, M5.5V secondary spectral type, Wade & Horne 1988; compared to $P_{orb} = 102.73 min$ for GD 552). Our search for the mass donor was thus a realistic and critical test for the suitability of HH1990's model.

There is a key point about our analysis that is worth emphasizing: we have managed to derive particularly strong constraints because of GD 552's relatively long orbital period which maximises the difference between the pre- and post-period-bounce systems. In particular it means that the mass donor in the pre-bounce model is relatively easy to detect, so that failure to detect it is a clear indication of the post-bounce alternative. We believe that this makes GD 552 one of the most secure post-period-minimum CV known (RE J1255+266 may be even better if its relatively long period can be confirmed, see Patterson et al. 2005). The method we employ is indirect, but necessarily so, since if the donor is a brown dwarf it is likely to contribute far less light than the upper limit we have derived.

It can be argued that there is also the possibility that GD552 is not a post-bounce system at all, even if its components are a WD with a brown dwarf donor. If GD552's progenitor was a binary composed of a main sequence star and a brown dwarf, instead of a double main sequence binary, it

would have evolved into the CV we see today without the need of going through the minimum period. We would not be able to distinguish between these two systems at all. Politano (2004) found that CVs that evolve directly to a short orbital period are expected to be rare because the progenitor systems containing a solar-type star and a brown dwarf are known to be rare ("the brown-dwarf desert").

5 CONCLUSIONS

We have used I-band spectroscopy in an attempt to detect the mass donor of the cataclysmic variable GD 552. Failure to detect the donor star puts strong limits on its mass, ruling out a main sequence nature.

We have shown GD 552 data to be consistent with a model in which its components are an ordinary white dwarf and a brown dwarf, at a moderate inclination angle. Population synthesis calculations favour the idea that the mass donor reached the stage of brown dwarf through evolution instead of being born as such. This suggests that GD 552 is likely to be a post-period minimum CV, making it the "period bouncer" with the longest securely-determined orbital period known.

We confirm the value obtained by HH1990 for the radial velocity semiamplitude of the white dwarf and determine for it a $T_{\rm eff}$ of 10900 ± 400 K by fitting the spectra with a grid of white dwarf models. The temperature determined for the white dwarf in GD552 is consistent with the red edge of the instability strip ($11\,000 < T_{\rm eff} < 12\,000$ K; Bergeron et al. 1995). From the 5.4 h stretch of photometry presented, we find no indication of the presence of pulsations. The lightcurve shows significant varibility but not with the periodicities and amplitudes characteristic of ZZ Cet stars.

ACKNOWLEDGMENTS

EU was supported by PPARC (UK) and Fundación Andes (Chile) under the program Gemini PPARC-Andes throughout most of this research. EU and RH-G were also supported by Universidad Católica del Norte's Proyecto de Investigación en Docencia 220401-10602015. TRM was supported under a PPARC SRF during some of the period over which this work was undertaken. LM-R is supported by NWO VIDI grant 639.042.201 to P. J. Groot. BTG was supported by a PPARC Advanced Fellowship.

The authors acknowledge the data analysis facilities provided by the Starlink Project which is run by the University of Southampton on behalf of PPARC. This research has made use of NASA's Astrophysics Data System Bibliographic Services. We acknowledge with thanks the variable star observations from the AAVSO International Database contributed by observers worldwide and used in this research.

The INT and the WHT are operated on the island of La Palma by the Isaac Newton Group in the Spanish Observatorio del Roque de los Muchachos of the Instituto de Astrofisica de Canarias This research was also partly based on observations made with the NASA/ESA Hubble Space Telescope, obtained from the data archive at the Space Telescope Science Institute. STScI is operated by the Association of Universities for Research in Astronomy, Inc. under NASA contract NAS 5-26555; these observations are associated wirh program 9406.

REFERENCES

Araujo-Betancor, S. et al., 2005, A&A 430, 629
Bessell, M., 1999, PASP 111, 1426
Bergeron P., Wesemael F., Lamontagne R., Fontaine G., Saffer R.A., Allard N.F., 1995, ApJ 449, 258
Cannizzo, J., 1993, ApJ 419, 318
Delfosse, X. et al., 2000, A&A 364, 217
Diaconis, P., Efron, B., 1983, Sci. Am., v. 248, n. 5, 96
Friend, M., Smith, R., Martin, J., Jones, D., 1988, MNRAS 233, 451
Gänsicke, B.T., Sion, E.M., Beuermann, K., Fabian, D., Cheng, F.H., Krautter, J., 1999, A&A 347, 178
Gänsicke, B.T., Araujo-Betancor, S., H.-J. Hagen, E.T. Harlaftis, S. Kitsionas, S. Dreizler, D. Engels, 2004, A&A 418, 270
Gänsicke, B.T., 2006, MNRAS, 365, 969
Gänsicke, B.T., Beuermann, K, Thomas, H.-C., 1997, MNRAS 289, 388
Gänsicke, B.T., Sion, E.M., Beuermann, K., Fabian, D., Cheng, F.H., Krautter, J., 1999, A&A 346, 151
Giclas, H., Burnham, R., Thomas, N., 1970, Lowell Obs. Bull. 153
Greenstein, J., Giclas, H., 1978, PASP 90, 460
Hamada, T., Salpeter, E., 1961, ApJ 134, 683
Hessman, F., Hopp, U., 1990, A&A 228, 387
Horne, K., Marsh, T., 1986, MNRAS 218, 761
Howell, S., Nelson, L., Rappaport, S., 2001, ApJ 550, 897
Hubeny, I, Lanz, T, 1995, ApJ 439, 875
Kirkpatrick, J., McCarthy, D., 1994, AJ 107, 333
Kirkpatrick, J., Henry, T., McCarthy, D., 1991, ApJS 77, 417
Kolb, U., 1993, A&A 271, 149
Kolb, U., Baraffe, I., 1999, MNRAS 309, 1034
Leggett, S., 1992, ApJS, 82, 351
Lin, D.N.C., Williams, R.E., Stover, R.J., 1988, ApJ 327, 234
Littlefair, S., Dhillon, V., Martin, E. , 2003, MNRAS 340, 264
Littlefair, S., Dhillon, V., Marsh, T., Gänsicke, B., Southworth, J., Watson, C., 2006, Science, 314, 1578
Lomb, N., 1976, Ap&SS 39, 447
Marsh, T.R., 1987, MNRAS 229, 779
Marsh, T.R., 1988, MNRAS 231, 1117
Marsh, T.R., 1989, PASP 101, 1032
Marsh, T.R., 1990, ApJ 357, 621
Marsh, T.R., Horne, K., 1988, MNRAS 235, 269
Mennickent, R. E., Diaz, M., Skidmore, W., Sterken, C., 2001, A&A 376, 448
Oke, J., 1990, AJ 99, 1621
Patterson, J., Thorstensen, J., Kemp, J., 2005, PASP 117, 427
Politano, M., 2004, ApJ 604, 817
Politano, M., Howell, S.B., Rappapport, S., 1998, in "Wild stars in the Old West.", Howell S., Kuulers E., Woodwards, C. (eds.), ASP Conference Series 137, p. 207
Putte, D., Smith, R., Hawkins, N., Martin, J., 2003, MNRAS 342, 151
Rodriguez-Gil, P., Gänsicke, B.T., Hagen, H.-J., Marsh, T.R., Harlaftis, E.T., Kitsionas, S., Engels, D., 2005, A&A 431, 269
Scargle, J., 1982, ApJ 263, 835
Schneider, D., Young, P., 1980, ApJ 238, 946
Shafter, A., Szkody, P., Thorstensen, J., 1986, MNRAS 308, 765
Sion, E., Szkody, P., 2005, in "White Dwarfs: Cosmological and Galactic Probes", Sion, E., Vennes, S., Shipman, H. (eds.), Astrophysics and Space Science Library 332, p. 217 ff.

Smak, J., 1981, Acta Astron. 31, 395
Smith, M., Dhillon, V., Marsh, T., 1998, MNRAS 296, 465
Southworth, J., Gänsicke, B., Marsh, T., de Martino, D., Hakala, P., Littlefair, S., Rodrguez-Gil, P., Szkody, P., 2006, MNRAS 373, 687
Szkody, P. et al., 2007, AJ 134, 185
van Zyl, L. et al., 2004, MNRAS 350, 307
Wade, B., Horne, K., 1988, ApJ 324, 411
Warner, B., Woudt, P.A., 2004, MNRAS 348, 599
Warner, B., Woudt, P.A., 2005, PASP 334, 453
Willems, B., Kolb, U., Sandquist, E., Taam, R., Dubus, G., 2005, ApJ 635, 1263
Williams, G., Shipman, H., 1988, ApJ 326, 738
Williams, R.E., 1980, ApJ 235, 939
Wilson, R., 1953, Carnegie Inst. Washington D.C. Publ. 601

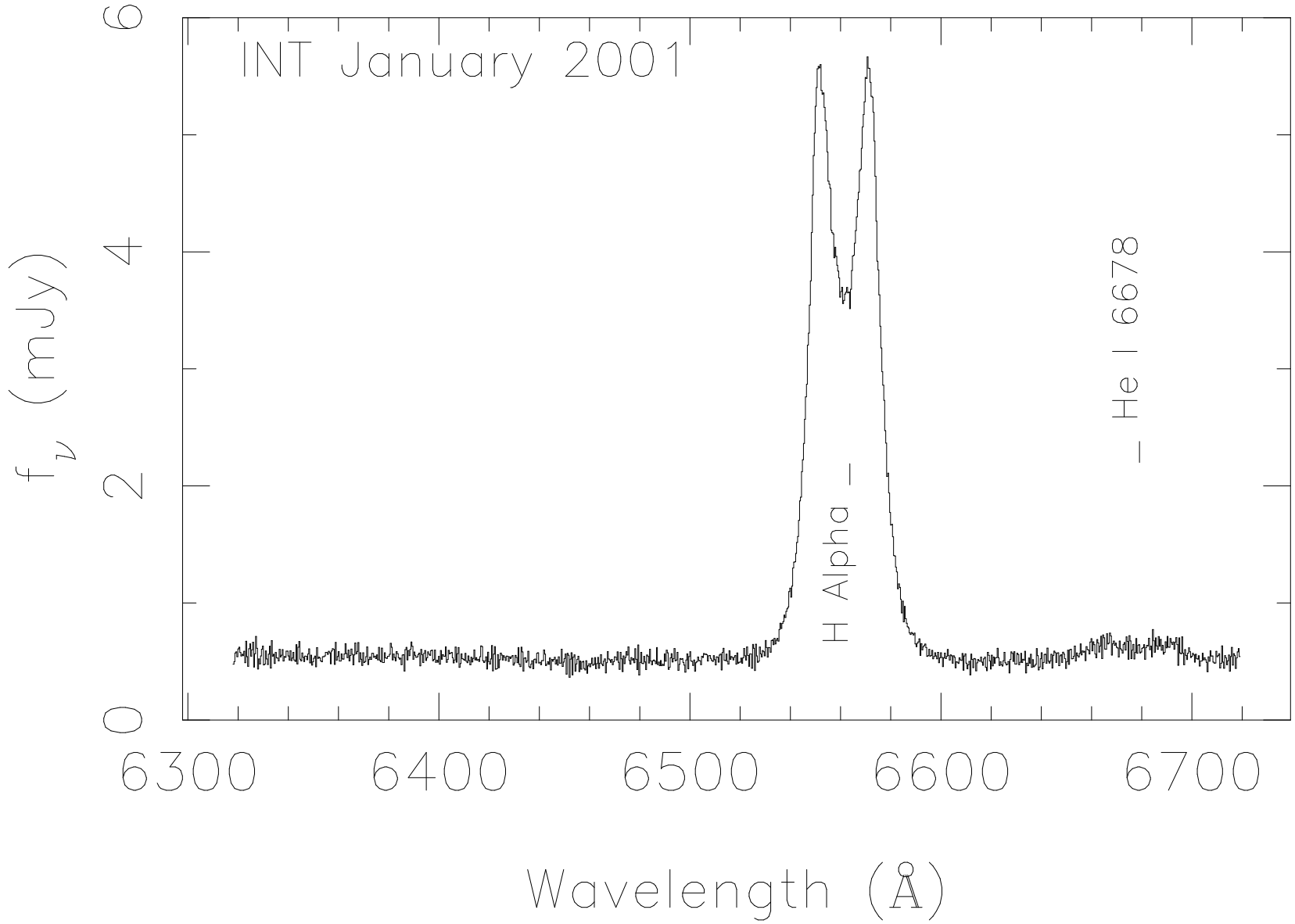
INT January 2001
H Alpha
He I 6678
f_ν (mJy)
0
2
4
6
6300
6400
6500
6600
6700
Wavelength (Å)

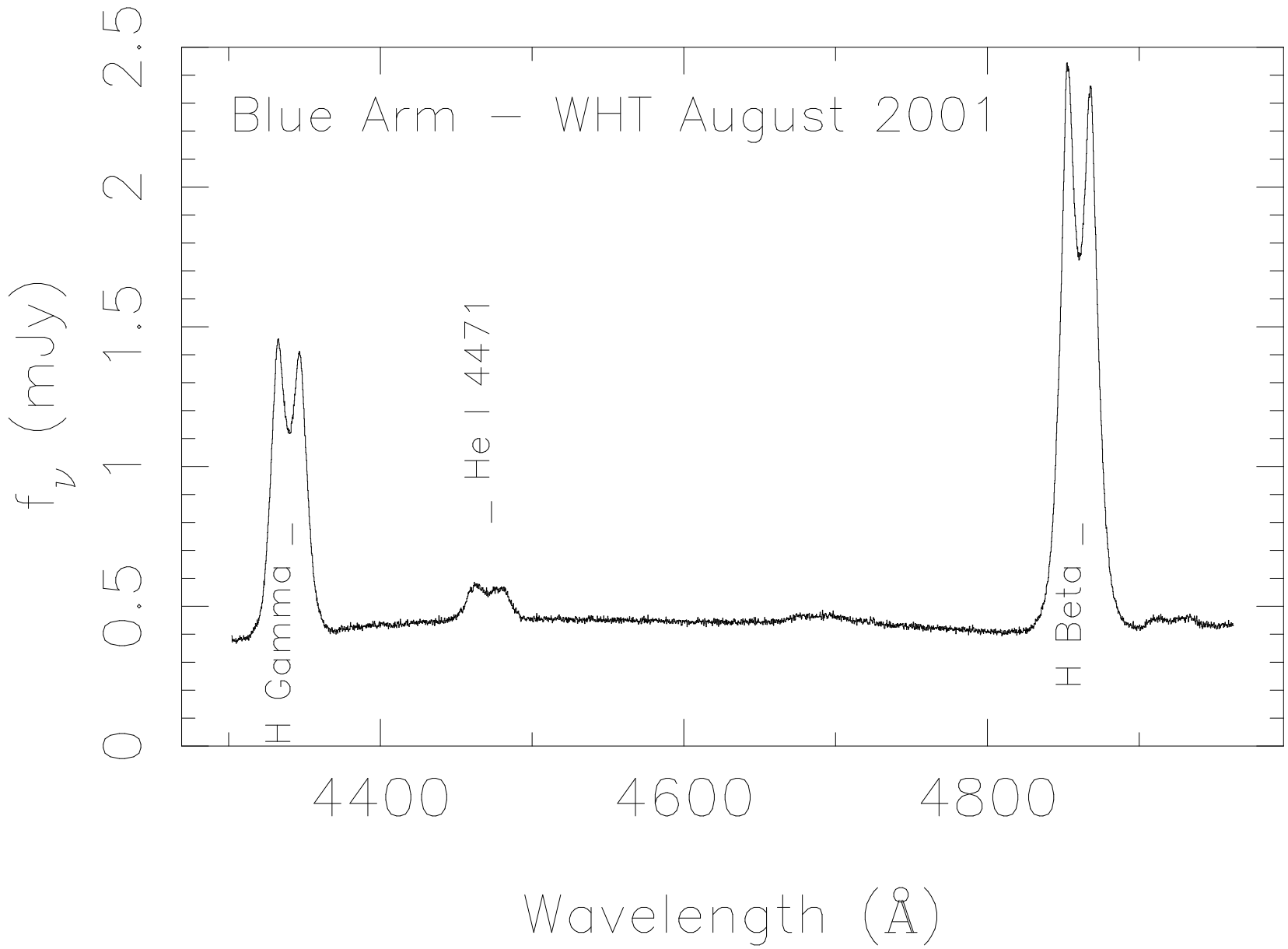
Blue Arm – WHT August 2001
H Gamma
He I 4471
H Beta
f_ν (mJy)
0
0.5
1
1.5
2
2.5
4400
4600
4800
Wavelength (Å)

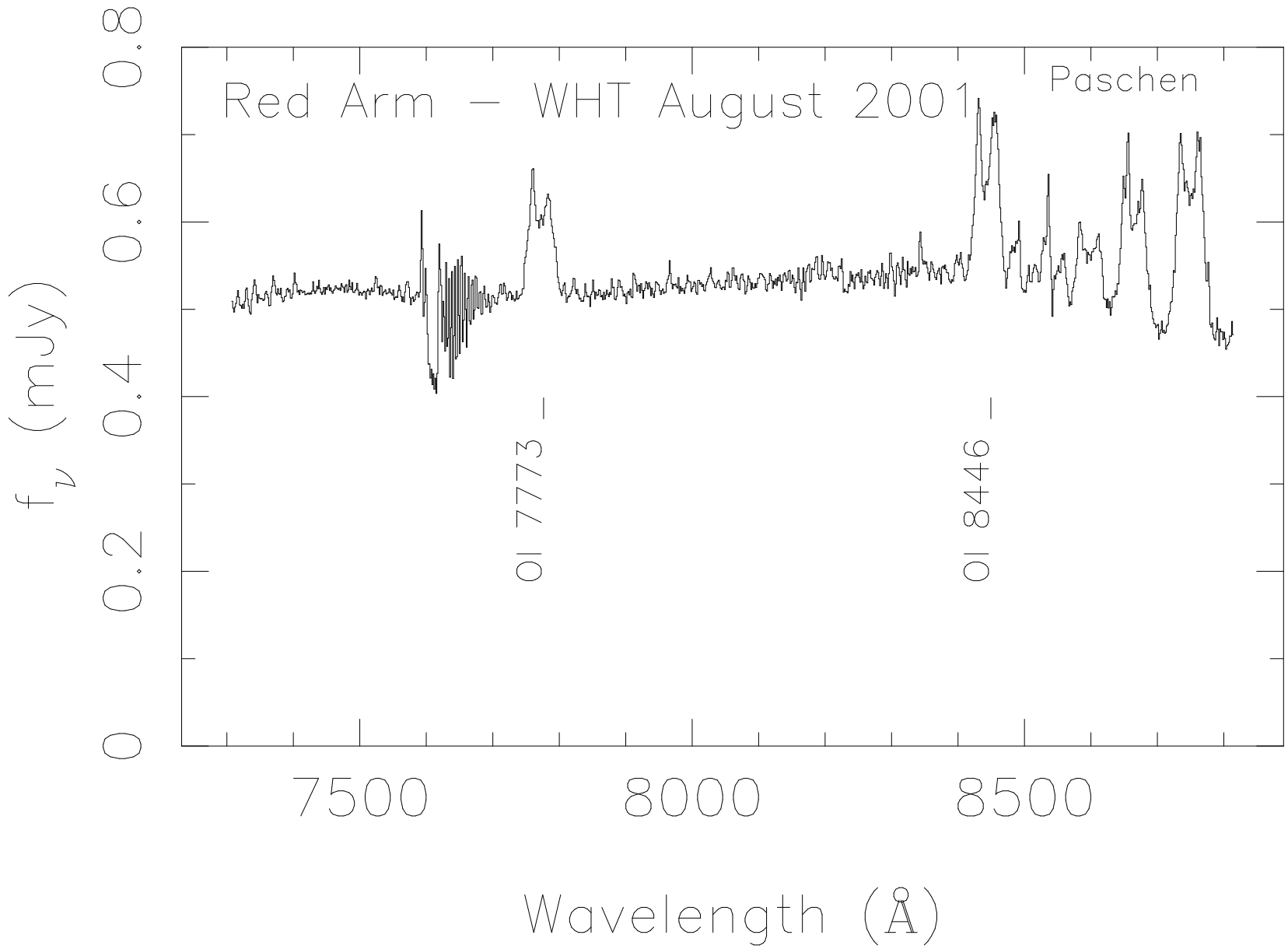
Red Arm – WHT August 2001
Paschen
OI 7773
OI 8446
0
0.2
0.4
0.6
0.8
f_ν (mJy)
7500
8000
8500
Wavelength (Å)

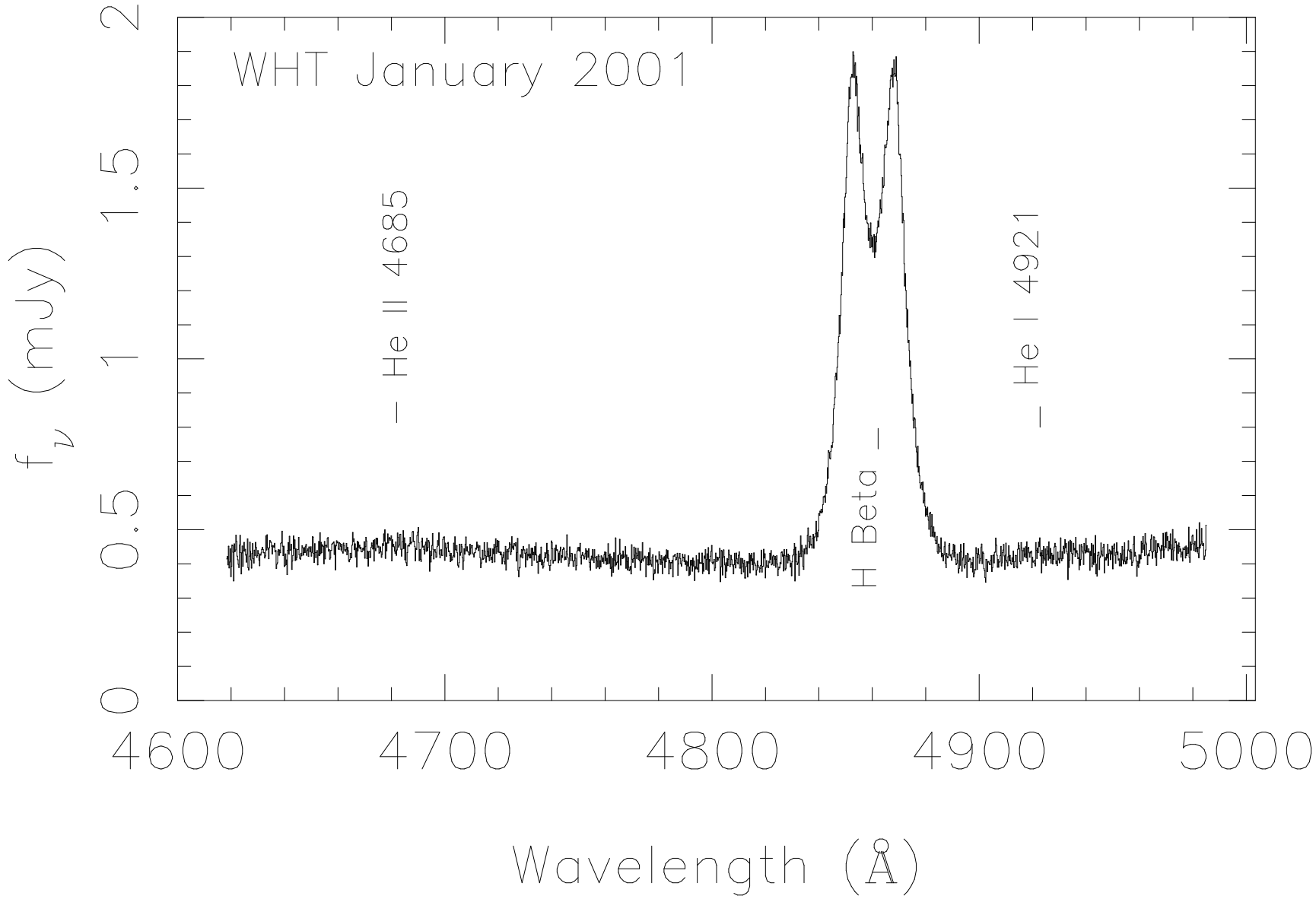
WHT January 2001
He II 4685
H Beta
He I 4921
f_ν (mJy)
0
0.5
1
1.5
2
4600
4700
4800
4900
5000
Wavelength (Å)

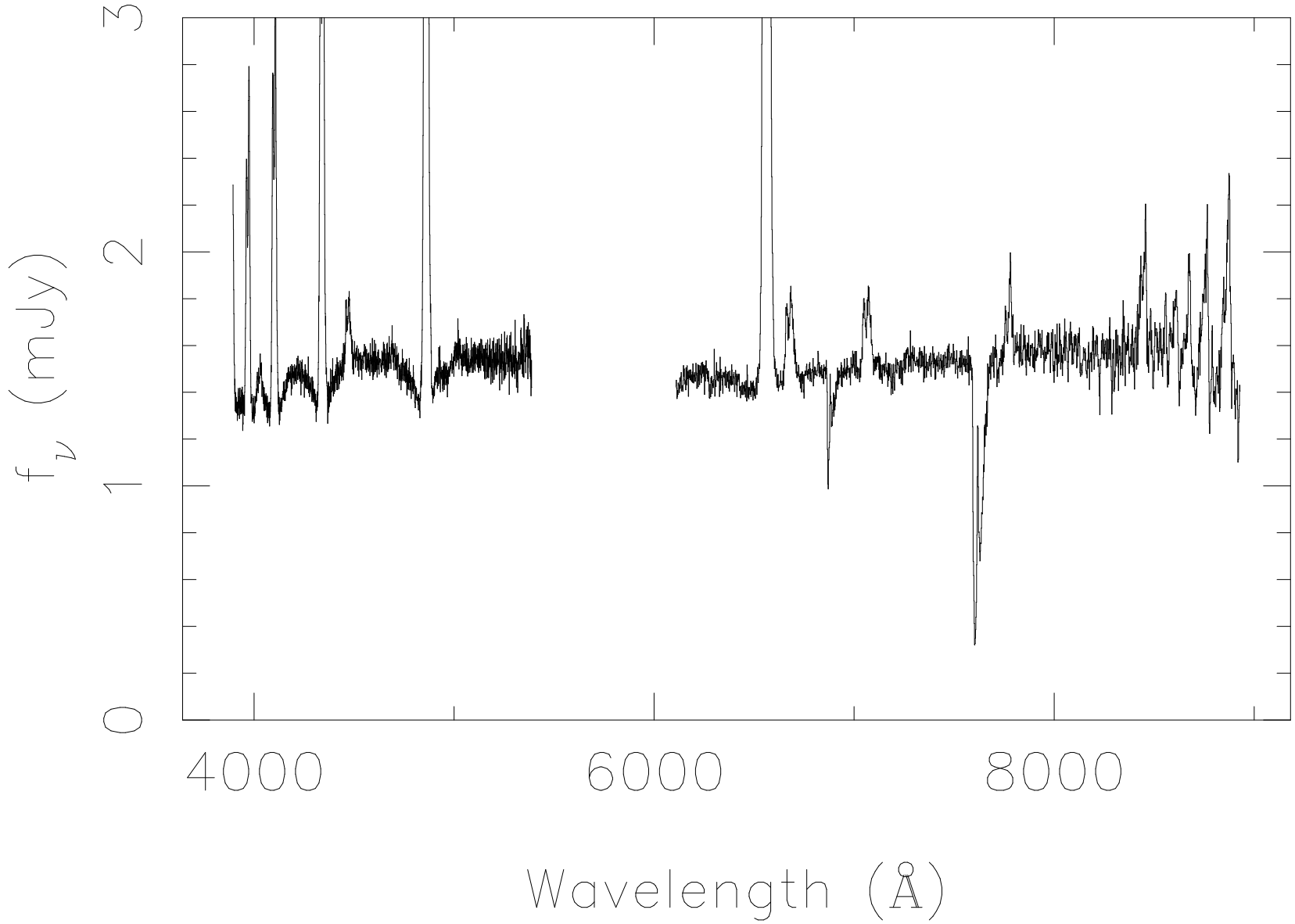
3
2
1
0
f_ν (mJy)
4000
6000
8000
Wavelength (Å)

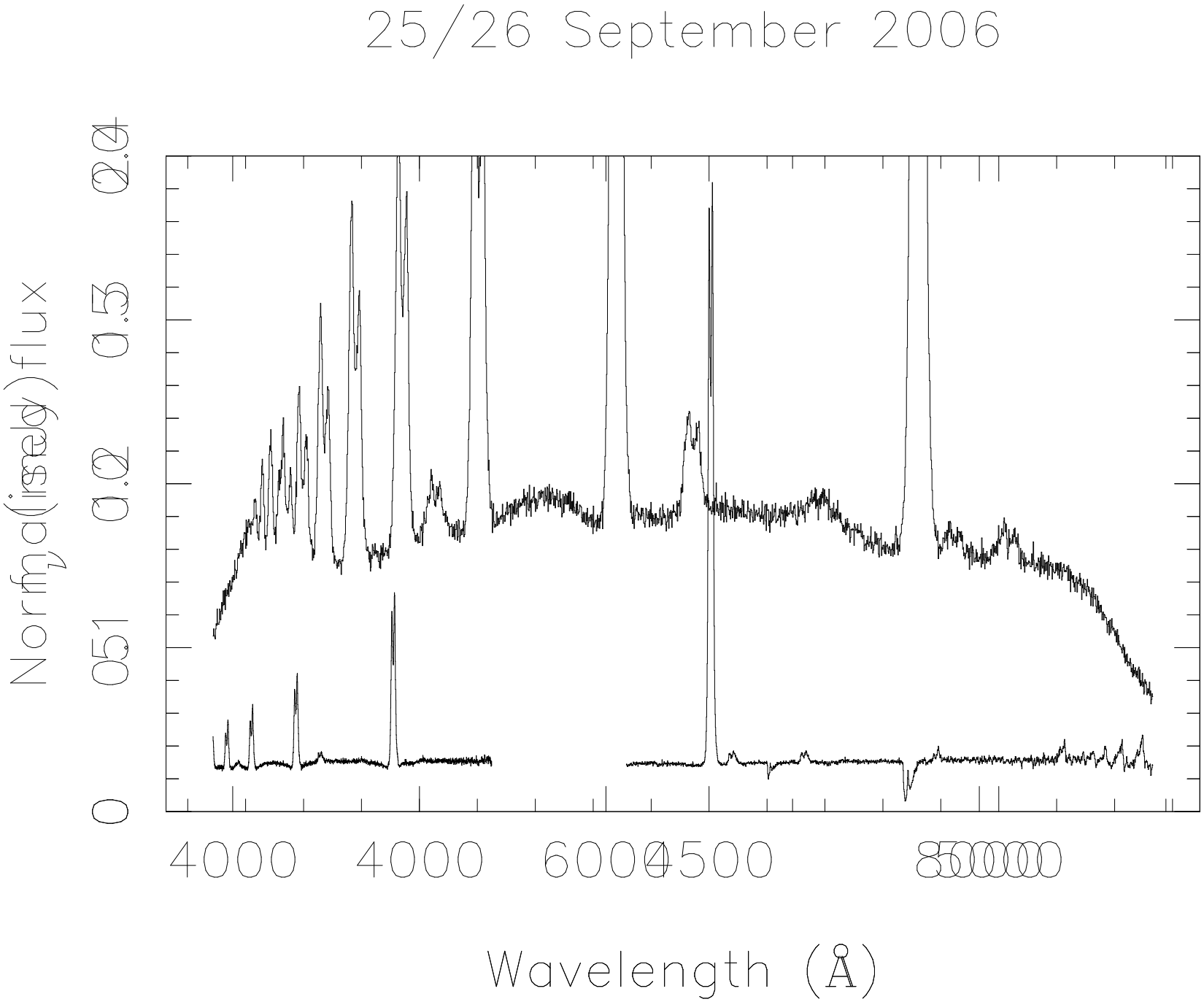
25/26 September 2006
Normalised flux
0
0.1
0.2
0.3
0.4
4000
4000
6000
4500
8500
Wavelength (Å)

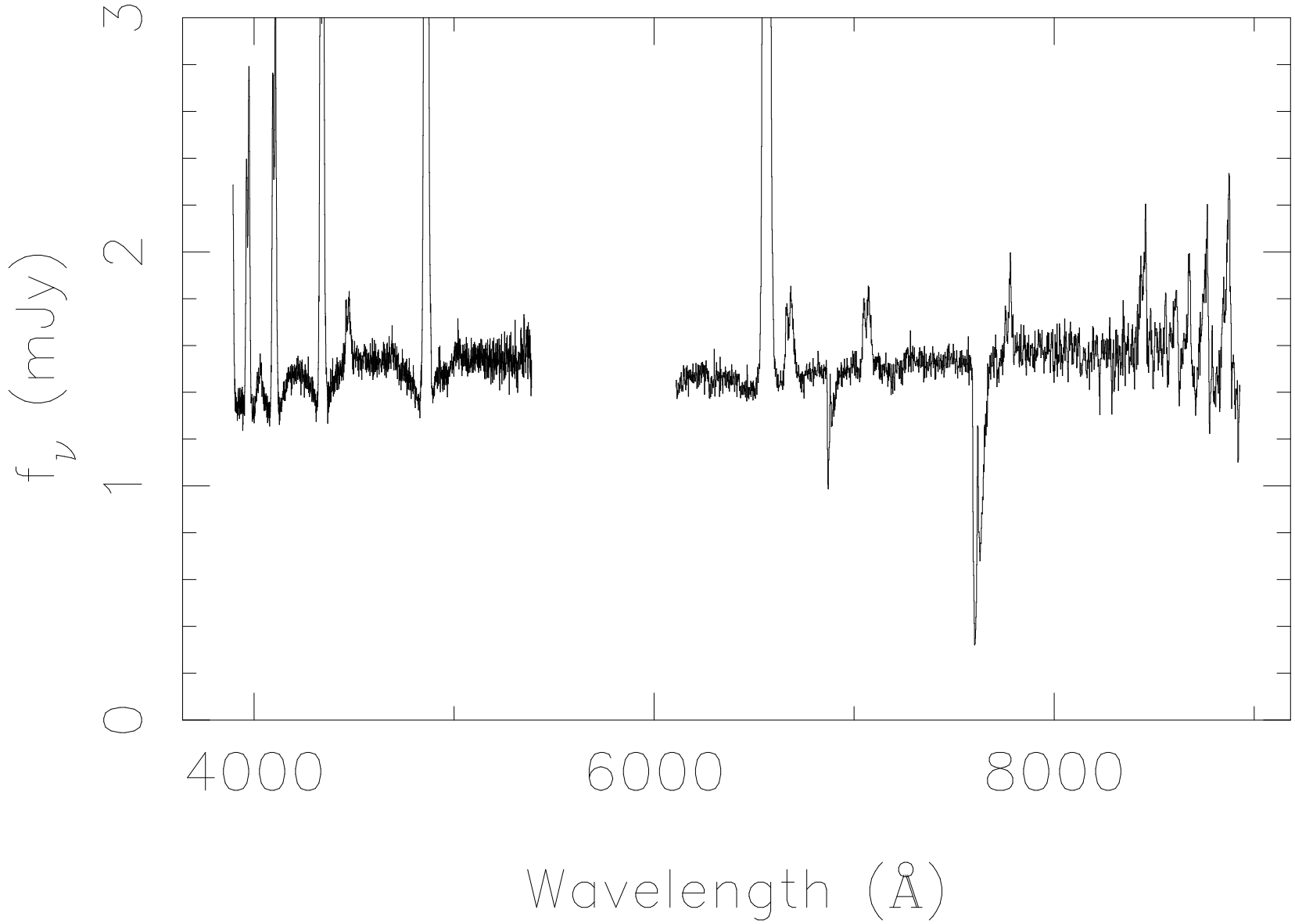
3
2
1
0
f_ν (mJy)
4000
6000
8000
Wavelength (Å)

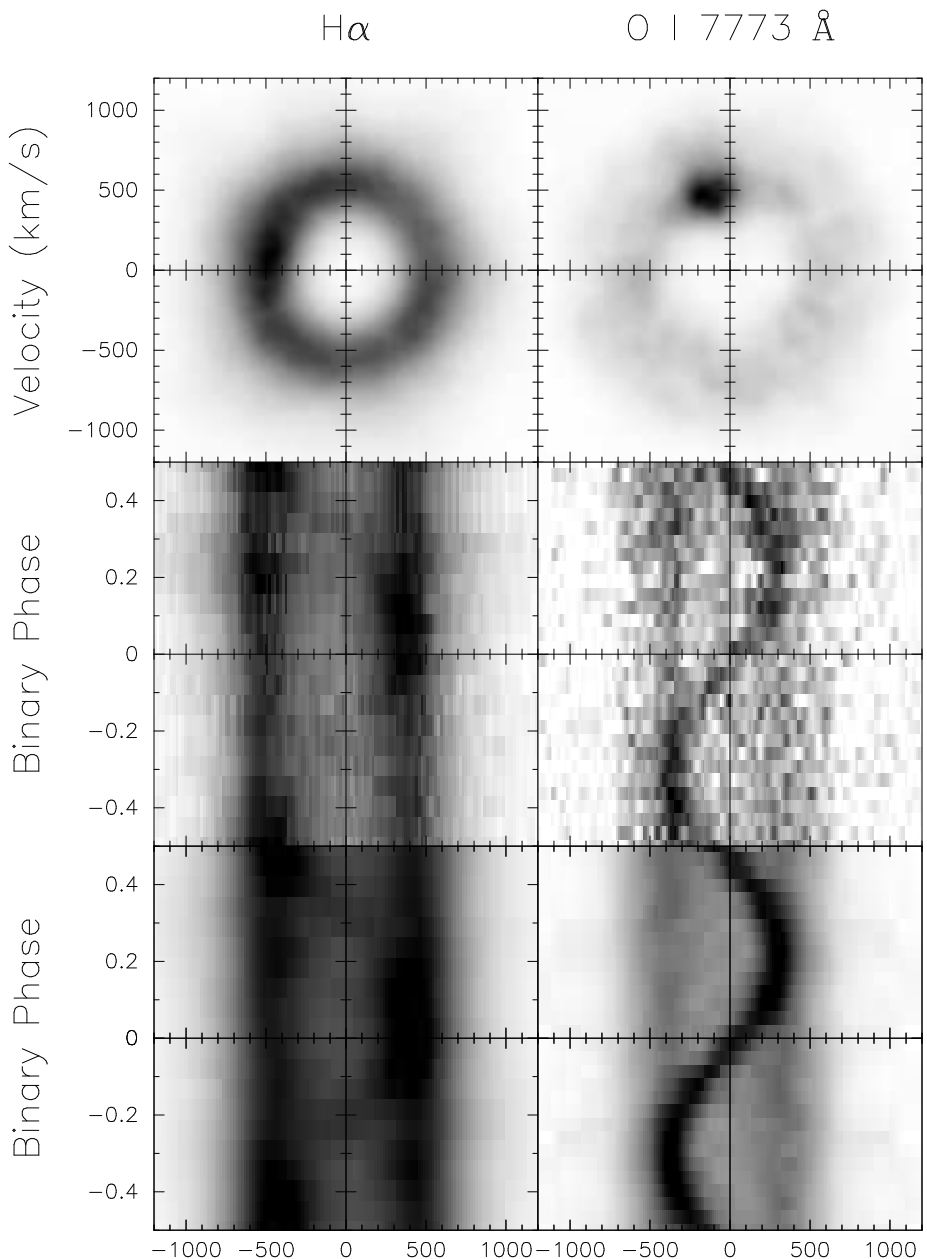
Hα
O I 7773 Å
Velocity (km/s)
1000
500
0
−500
−1000
Binary Phase
0.4
0.2
0
−0.2
−0.4
Binary Phase
0.4
0.2
0
−0.2
−0.4
−1000 −500 0 500 1000
−1000 −500 0 500 1000